Available online at www.sciencedirect.com

ScienceDirect

Journal of Computational and Applied Mathematics 199 (2007) 141 – 148

JOURNAL OF COMPUTATIONAL AND APPLIED MATHEMATICS

www.elsevier.com/locate/cam

# Local algorithms in exterior tomography

Eric Todd Quinto

*Department of Mathematics, Tufts University, Medford, MA 02155, USA*

Received 17 August 2004; received in revised form 27 November 2004

**Abstract**

Exterior tomographic data are taken over lines outside a central region, and such data occur in the industrial nondestructive evaluation of large objects such as rockets. We explain, using microlocal analysis, which singularities are well reconstructed from exterior data, and we explain how this phenomenon is reflected in the singular value decomposition for the exterior transform [E.T. Quinto, Singular value decompositions and inversion methods for the exterior Radon transform and a spherical transform, J. Math. Anal. Appl. 95 (1983) 437–448]. We extend Lambda Tomography to exterior data and to limited angle exterior data. The algorithm is tested on industrial data from Perceptics, Inc.



*Keywords:* Limited data tomography; Exterior Radon transform; Lambda Tomography; Microlocal analysis

## 1. Introduction

Tomography has revolutionized diagnostic medicine and industrial nondestructive evaluation. Doctors can see the internal structure of the body and researchers can noninvasively discover cracks in rockets. X-ray tomography is based on the transform created by Johann Radon in 1917 [29] that integrates functions over lines. To describe the transform, we parameterize lines by $(\omega, p) \in [0, 2\pi] \times \mathbb{R}$, and $\ell(\omega, p) = \{x \in \mathbb{R}^2 \,|\, x \cdot \overline{\omega} = p\}$, is the line perpendicular to $\overline{\omega} = (\cos\omega, \sin\omega)$ and containing $p\overline{\omega}$. The Radon transform of $f \in L^1(\mathbb{R}^2)$ is

$$Rf(\omega, p) = \int_{x \in \ell(\omega, p)} f(x)\, \mathrm{d}s.$$

In practical applications, data are given over only a finite number of lines. Roughly speaking, *complete data* are data over a fairly evenly spaced set of lines in fairly evenly distributed directions. Effective and fast reconstructions algorithms for complete data (e.g., [19,20]) produce useful reconstructions (images of the object being scanned).

Some of the most interesting problems in tomography are *limited data problems*, for which some data are missing. Since the standard algorithms require complete data, different algorithms are needed. We provide algorithms for two limited data problems, *the exterior problem* in which line integrals are given over lines exterior to a central region, and *the limited angle exterior problem* in which exterior tomography data are given over lines in a limited angular range.

The exterior problem came up in the early days of medical tomography. Early X-ray scanners were so slow that the beating of the heart would create artifacts in the scan, and doctors wanted to image the exterior of the heart, anyway,

*E-mail address:* Todd.Quinto@tufts.edu
*URL:* http://www.tufts.edu/∼ equinto.

0377-0427/$ - see front matter © 2005 Elsevier B.V. All rights reserved.
doi:10.1016/j.cam.2004.11.055

so they had exterior data. This is no longer a problem since modern scanners take data quickly enough to stop the movement of the heart. However, the exterior problem is important in industrial tomography of large objects such as rocket bodies [33]. X-rays cannot penetrate the center of large rocket bodies and turbines, but they do penetrate the parts exterior to this center region. Engineers need to know whether there are cracks, or other defects in the outer shell or bubbles between the shell and fuel insulation.

Nobel Laureate and tomography pioneer Allan Cormack developed an inversion formula that solved the exterior problem [4], but it was numerically unstable and he developed and tested a singular value decomposition inversion method for complete data [5]. In fact, the exterior problem is highly ill-posed, and the instability is a part of the problem, as we will see in Section 2. Bates and Lewitt [1] developed a data completion method for this problem, and Frank Natterer [18] developed a regularization method. Inspired by Allan Cormack, who was a mentor, the author developed a singular value decomposition for this problem [25] (see Perry [21] for $\mathbb{R}^2$). This decomposition includes a null space, and the author developed a bounded extrapolation procedure to approximate the null component of compactly supported functions [26].

Limited angle tomography comes up in areas such as luggage testing in which one can take a limited range of views of the object. Algorithms have been developed by researchers [6,13,14,17,30]. A limited angle Lambda Tomography algorithm was given in [12]. A related algorithm has been developed by the author and tested on electron microscope data from the Karolinska Institute and Sidec Technologies (unpublished). *The limited angle exterior problem* comes up when the object to be scanned is so large that only exterior data are available and when one can get exterior data from only one side of the object. Each of these reconstruction methods provides worse reconstructions than the standard algorithms would if the complete data were given; some singularities (e.g., boundaries of regions) are less well reconstructed than others.

In Section 2, we will describe the singular value decomposition for the exterior problem and relate it to the microlocal analysis of singularities for this problem. In Section 3 we will give a short overview of Lambda Tomography, and then in Section 4 we present our extension algorithm. Reconstructions from industrial data provided by Perceptics, Inc., and discussion are in Section 5.

## 2. Singularities and the singular value decomposition for the exterior transform

In this section, we will define singularities rigorously and explain the singularities of objects that are visible from exterior data. Then we will show how this phenomenon is reflected in the author's singular value decomposition [25] and his original exterior reconstruction algorithm [26,28].

The Fourier transform of $f \in L^2(\mathbb{R}^n)$ is defined

$$(\mathscr{F} f)(\xi) = \int_{x\in\mathbb{R}^n} \mathrm{e}^{-\mathrm{i}x\cdot\xi} f(x)\,\mathrm{d}x \quad \text{and} \quad f(x) = \frac{1}{(2\pi)^n}\int_{\xi\in\mathbb{R}^n} \mathrm{e}^{\mathrm{i}x\cdot\xi}(\mathscr{F} f)(\xi)\,\mathrm{d}\xi. \tag{2.1}$$

Practically, singularities are density jumps, or boundaries between regions, and mathematically they occur at points where the density of the object is not smooth. To make this rigorous, we recall that a function $f$ has $s$ Sobolev derivatives ($f \in H^s(\mathbb{R}^n)$) if and only if $\mathscr{F} f \in L^2(\mathbb{R}^n, (1+\|\xi\|^2)^s)$. In order to capture local Sobolev information, we localize $f$ at $x_0 \in \mathbb{R}^n$ by multiplying $f$ by a smooth compactly supported cut-off function $\varphi$ ($\varphi(x_0) \neq 0$). Then we ask whether this localized Fourier transform, $\mathscr{F}(\varphi f)$, is in $L^2(\cdot, (1+\|\xi\|^2)^s)$ near a specified direction. This leads to the definition.

**Definition 1** (*Petersen [22]*). Let $x_0 \in \mathbb{R}^n$ and $\xi_0 \in \mathbb{R}^n\backslash 0$. The function $f$ *is in* $H^s$ *at* $x_0$ *in direction* $\xi_0$ *iff* there is a smooth, compactly supported cut-off function $\varphi \in C_c^\infty(\mathbb{R}^n)$ with $\varphi(x_0) \neq 0$, and an open cone $V$ containing $\xi_0$ such that

$$\mathscr{F}(\varphi\, f)(\xi) = \int_{x\in\mathbb{R}^n} \mathrm{e}^{-\mathrm{i}x\cdot\xi}\varphi(x)\, f(x)\,\mathrm{d}x \tag{2.2}$$

is in $L^2(V, (1+\|\xi\|^2)^s)$ ($f$ is said to be in $H^s$ near $x_0$ *iff* $V$ can be taken to be all of $\mathbb{R}^n$). On the other hand, $(x_0, \xi_0)$ is in the $H^s$*-wavefront set*, $\mathrm{WF}^s(f)$, *iff* $f$ is *not* in $H^s$ at $x_0$ in direction $\xi_0$.

As an example, if $f$ is 1 inside a circle in the plane and 0 outside, then $\mathrm{WF}^0(f) = \emptyset$ since $f \in L^2$ but $\mathrm{WF}^{1/2}(f)$ is the set of normal vectors to the circle. Note that the wavefront set is typically defined as a subset of the cotangent

bundle so it is invariant under coordinate changes, but in $\mathbb{R}^n$, we will consider $\xi$ as a tangent vector. We can define the wavefront set for functions on lines as in definition (2.2) because the cut-off function $\varphi(\omega, p)$ localizes in $\omega$ as well as in $p$ (and we extend at the endpoints periodically in $\omega$).

In the article [27], the author used the microlocal analysis of the Radon transform to explain what the Radon transform does to singularities.

**Theorem 2** (*Quinto [27, Theorem 3.1]*). *Let $f$ be a distribution of compact support. There is a one-to-one correspondence between the $H^s$ wavefront set of $f$ and the $H^{s+1/2}$ wavefront set of Rf. Let $\omega_0 \in [0, 2\pi]$, $p_0 \in \mathbb{R}$, and $x_0 \in \ell_0 = \ell(\omega_0, p_0)$.*

$$(x_0; \overline{\omega}_0) \in \mathrm{WF}^s(f) \quad \textit{iff} \quad ((\omega_0, p_0); ((-\omega_0^{\perp} \cdot x), 1)) \in \mathrm{WF}^{s+1/2}(Rf), \tag{2.3}$$

*where $\omega^{\perp} = (-\sin\omega, \cos\omega)$.*

*Therefore, if for some $x_0 \in \ell_0$, $(x_0, \overline{\omega}_0) \in \mathrm{WF}^s(f)$, then Rf is not in $H^{s+1/2}$ near $\ell_0$. If $f$ is $H^s$ in directions $\pm\overline{\omega}_0$ at every point on $\ell_0$, then Rf is in $H^{s+1/2}$ near $\ell_0$. Undetected singularities (those not perpendicular to the line being integrated over) are smoothed by $R$.*

This theorem is true because $R$ is an elliptic Fourier integral operator [10,24] and Fourier integral operators transform wavefront sets in precise ways [11]. Candès and Demanet [2] have developed a curvelet theory of Fourier integral operators and wavefront sets that could provide a way of directly calculating the wavefront set of Radon data, *Rf*, and then using Theorem 2 to detect singularities of $f$ from this data.

The theorem has several implications for limited data tomography. First, the Radon transform, $R$, with limited data does a good job detecting a singularity of $f$ when the line is perpendicular to the singularity (e.g., the line is tangent to a boundary of part of the object). If a singularity of the function $f$ in $H^s$ is perpendicular to the line $\ell_0$, then *Rf* will have a singularity in a corresponding direction at $\ell_0$ of order $s + \frac{1}{2}$. Second, if a singularity is not perpendicular to any line in the data set, then it is smoothed to $C^{\infty}$ by the data and will be harder to reconstruct stably.

Putting these together, we see that if $\ell_0$ is a line in a data set, then singularities of $f$ perpendicular to $\ell_0$ will be visible, but other singularities are smoothed. The reconstruction in Fig. 1, from the author's exterior reconstruction algorithm [26], illustrates this perfectly. The lines in the data set are those that do not meet the center disk, and the boundaries tangent to those lines (with wavefront perpendicular to those lines) are better defined than other parts of the boundaries. That is, for each circle, the inside and outside boundaries are better defined than the sides.

This analysis also explains why the exterior problem is highly ill-posed. $R$ smooths undetected Sobolev singularities to $C^{\infty}$ so the inverse cannot be continuous in any range of Sobolev norms.

We will now show how the singular value decomposition for the exterior problem reflects the same phenomenon about singularities. Let $E = \{x \in \mathbb{R}^2 \mid \|x\| \geqslant 1\}$; $E$ represents the area to be reconstructed, and let $E' = \{(\omega, p) \mid \omega \in [0, 2\pi],\ p \geqslant 1\}$ be the set of lines contained in $E$, those in the exterior data set.

The SVD is explicitly given in [26], and its salient properties are described now. We consider the transform $R : L^2(E, \|x\|(1 - \|x\|^{-2})) \to L^2(E', 1/p\,\mathrm{d}\omega\,\mathrm{d}p)$ and define singular functions $\{f_{\ell m}\}$ on the domain and $\{g_{\ell m}\}$ on the image:

$$Rf_{\ell m} = c_{\ell m} g_{\ell m} \quad c_{\ell m} = \begin{cases} 0 & m < |\ell| \\ \mathcal{O}(1/\sqrt{m}) & m \geqslant |\ell| \end{cases}$$
$$\text{where} \quad f_{\ell m}(r, \theta) = Q_m(r^{-1}) \mathrm{e}^{\mathrm{i}\ell\theta} \text{ in polar coordinates,} \tag{2.4}$$

$\ell \in \mathbb{Z}$, $m = 0, 1, \ldots, m + \ell$ is even, and $Q_m$ is a polynomial of degree $m + 2$ and parity of $\ell$. $Q_m$ is a normalized shifted Jacobi polynomial in $r^{-2}$ times $r^{-3}$ ($m$ odd) or $r^{-2}$ ($m$ even). The author's algorithm then uses a bounded extrapolation procedure to recover the null component using the fact $f$ has compact support.

The main point to be gleaned from (2.4) is that the functions in the null space oscillate more in $\theta$ than in $r$ (as $m < |\ell|$ for null functions in (2.4)) and those in the orthogonal complement of the null space oscillate more in $r$ than in $\theta$ as $m \geqslant |\ell|$ in (2.4). This perfectly corresponds to the microlocal predictions and it is illustrated in the reconstruction in Fig. 1, since the boundaries in the radial direction (inner and outer boundaries) are better imaged than those in the angular direction (the sides).

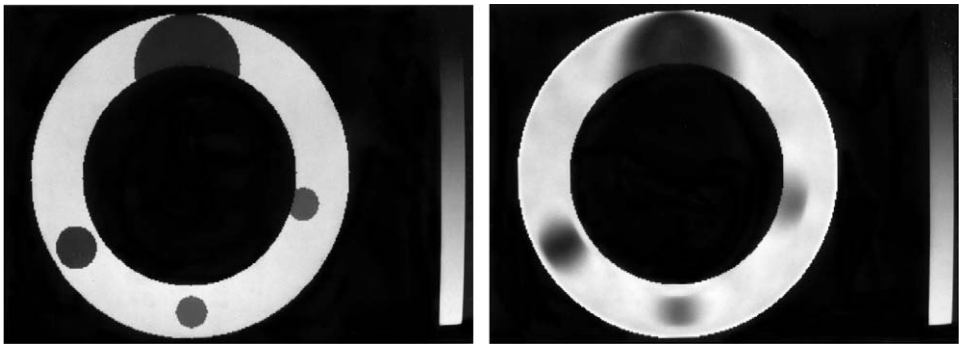

Fig. 1. Object (left) and reconstruction (right) from simulated data [26] using the author's exterior reconstruction algorithm.

## 3. An overview of Lambda Tomography

Before we describe our refinements, we will give an outline of Lambda Tomography [7–9,23,35]. The Lambda operator acts on Schwartz distributions

$$\Lambda_x f = \sqrt{-\Delta} f = \frac{1}{4\pi^2} \int_{\xi\in\mathbb{R}^2} e^{i\xi\cdot x} \|\xi\| \mathscr{F} f(\xi)\, d\xi, \tag{3.1}$$

and the key formula is

$$\Lambda_x f = \frac{-1}{4\pi} R^* \left( \frac{d^2}{dp^2} Rf \right), \tag{3.2}$$

where $R^*g(x) = \int_0^{2\pi} g(\omega, x\cdot\overline{\omega})\, d\omega$ is the dual Radon transform.

Standard Lambda Tomography is used for the *region of interest* (*ROI*) *problem*, in which the only data are over lines intersecting a region of interest. Although inversion is not possible for ROI data (e.g., [15]), all singularities are visible from ROI data [27]. Because Lambda Tomography reconstructs $\Lambda_x f$ (3.1) and $\Lambda_x$ is an elliptic pseudodifferential operator of order one with radial symbol, a Lambda reconstruction will accentuate all boundaries and singularities but not mask or "move" them.

Lambda Tomography is of filtered back projection type using a local filter (an approximation to the local operator $d^2/dp^2$). Because of this local filter and because $R^*g(x)$ integrates only over lines through $x \in \mathbb{R}^2$, this reconstruction method needs only data on lines near $x \in \mathbb{R}^2$ to reconstruct $\Lambda_x f(x)$. This is why Lambda Tomography is used for the region of interest problem.

We should point out that there are other inversion methods for region of interest tomography. Candès and Donoho [3] have developed ridgelets, which are an elegant generalization of regular wavelets that provides directionality, and they have adapted them to Radon inversion. This method, like the standard wavelet methods [32], provides local reconstruction algorithms for tomography. Ramm and Katsevich [31] have developed pseudolocal tomography, and Madych [16] has shown that these methods can be related using wavelets.

The data in most modern scanners are not taken on a set of lines parameterized by $(\omega, p)$ but on a fan beam grid and the corresponding transform is the *Divergent Beam Transform*:

$$Df(a,\theta) = \int_{t=0}^{\infty} f(a+t\theta)\, dt, \tag{3.3}$$

where $f \in L^1(\mathbb{R}^2)$, $a \in \mathbb{R}^2$ is the source of X-rays and $\theta \in S^1$ is the direction from $a$ of one of the X-rays used in the data set. In most planar fan beam scanners, an X-ray source moves in a circle around the object and the source

sends out a fan-shaped beam of X-rays. If the circle of sources has radius $S$, then we parameterize the set of sources by $\alpha \mapsto c(\alpha) = S(\cos\alpha, \sin\alpha)$ for $\alpha \in [0, 2\pi]$.

For each source $c(\alpha)$, and each direction $\theta \in S^1$, we let $\varphi$ represent the clockwise angle between the vectors $\theta$ and $-c(\alpha)$. This gives $\theta(\alpha, \varphi) = -(\cos(\alpha - \varphi), \sin(\alpha - \varphi))$ and it allows one to parameterize the divergent beam transform

$$\mathscr{D}f(\alpha, \varphi) = Df(c(\alpha), \theta(\alpha, \varphi)) = \int_{t=0}^{\infty} f(c(\alpha) + t\theta(\alpha, \varphi))\, \mathrm{d}t. \tag{3.4}$$

If $x$ is a point inside the circle of sources, we let $\tau$ be the clockwise angle between $-c(\alpha)$ and $(x - a)$, so $(x - a) = -\|x - a\|(\cos(\alpha - \tau), \sin(\alpha - \tau))$.

Kennan Smith [34] had the important insight that, rather than solving for $f$, one should solve for some approximation to $f$ that shows the salient features of the object. If $e_r(x)$ is an approximate identity, the goal is to solve for $(e_r) * f$ rather than $f$. Filtered back projection lends itself to this since the approximation specifies the convolution kernel in the inversion formula [34]. Typically, $e_r$ is a radial function, and in [8,9] they use

$$e_r(x) = r^{-2}e(x/r) \quad \text{where } e(x) = \begin{cases} \dfrac{2m+3}{2\pi}(1 - \|x\|^2)^{m+1/2} & \|x\| \leqslant 1, \\ 0 & \|x\| > 1, \end{cases} \tag{3.5}$$

and $m = 11.4174$ in our experiments, as suggested by Kennan Smith.

Then using this notation, Faridani, Smith, et al. [8,9] derived the divergent beam formula equivalent to (3.2):

$$(\Lambda_x\, e_r) * f(x) = \frac{S}{4\pi} \int_{\alpha=0}^{2\pi} \int_{\varphi=-\pi/2}^{\pi/2} \mathscr{D}f(\alpha, \varphi)\, \cos\varphi\, K_r(\|x - a\| \sin(\tau - \varphi))\, \mathrm{d}\varphi\, \mathrm{d}\alpha, \tag{3.6}$$

where

$$K_r(p) = r^{-3}K(p/r) \quad \text{where } K(p) = \begin{cases} C_m(1 - p^2)^{m-1}(1 - (2m+1)p^2) & |p| \leqslant 1, \\ 0 & |p| > 1, \end{cases} \tag{3.7}$$

where the constant $C_m = 2\Gamma(m + (\frac{5}{2}))/(\Gamma(m+1)\sqrt{\pi})$. In fact, $K_r$ is the second derivative in $p$ of the Radon transform of $(-e_r)$ [9]. Note that if $f$ is smooth enough, $(\Lambda_x\, e_r) * f = e_r * (\Lambda_x\, f)$ and so, since $e_r$ is an approximate identity, (3.6) is an approximation to $\Lambda_x\, f$.

By the definition of $K_r$, (3.7),

$$K_r(\|x - a\| \sin(\tau - \varphi)) = \|x - a\|^{-3}\, K_s(\sin(\tau - \varphi)) \quad \text{where } s = r/\|x - a\|.$$

A simplification (originally done by Lakshminarayanan for filtered back projection) is to assume that $\|x - a\|$ is constant for $x \in \operatorname{supp} f$, so $s = r/\|x - a\|$ is constant. This is a reasonable approximation, and for our reconstructions, the radius of the circle of sources, $S$, is at least three times as big as the radius of the object to be scanned. This gives [9, (9.4)]

$$(\Lambda_x\, e_r) * f(x) \sim \frac{S}{4\pi} \int_{\alpha=0}^{2\pi} \|x - a\|^{-3} \int_{\varphi=-\pi/2}^{\pi/2} \mathscr{D}f(\alpha, \varphi) \cos\varphi K_s(\sin(\tau - \varphi))\, \mathrm{d}\varphi\, \mathrm{d}\alpha, \tag{3.8}$$

and this allows one to calculate $K_s$ for a fixed $s$ rather than variable $s$. In practice the inner integral in (3.8) is calculated (for each $\alpha$) for equally spaced $\tau$ and then interpolated to other values as needed to evaluate (3.8) at each $x$.

## 4. Extending Lambda Tomography to exterior data

Regular Lambda Tomography cannot be applied to our problem since exterior data do not include all lines in the region of interest, the annulus, but only those exterior to the inner circle. We perform a data completion method, which will now be described, to allow the Lambda algorithm to be used. If using an inversion formula for the divergent

beam transform with complete data, we would extend in the range of the divergent beam transform, since it is the most effective method for standard inversion methods (see [1,13] for parallel beam data). However, one advantage of Lambda Tomography is that it reconstructs shapes of objects using local data, but it is not an inversion method. So, in general, any extension that does not create or destroy singularities is worth trying.

The data for Fig. 2 are standard fan-beam exterior tomography data of an annulus with inner radius 0.9532 if the outer radius is 1.0. Using parameterization (3.4), we have data $\mathscr{D}f(\alpha, \varphi)$ for $\alpha \in [0, 2\pi]$ but only for $\varphi \in [\phi_0, \phi_1]$ where $\phi_0$ is the angle between the origin, $a(\alpha)$, and the tangent to the inner circle, and $\phi_1$ is the angle to the outer circle of the annulus. So, to use (3.8), the data need to be extended from $[\phi_0, \phi_1]$ to $[-\phi_1, \phi_1]$. The author tried several methods. First, as was done in [12] and unpublished work for limited angle Lambda Tomography, we extended the data smoothly to zero in $[-\phi_1, \phi_0]$. This gives slightly worse reconstructions near the inner boundary than the method we eventually used, probably because it creates a jump singularity at the inner boundary.

The method we use averages $\mathscr{D}f(\alpha, \varphi)$ near $\varphi = \phi_0$ (the innermost 3% of detectors) and then smoothly extends the data inside by this average value. Our extension in effect makes the derivative equal to zero on the extended range, $[-\phi_1, \phi_0]$, and the transition at the inner boundary is smoother than extending the data itself by zero which creates a jump at the inner boundary.

The reconstruction in Fig. 3 is from limited angle exterior data. Using parameterization of (3.4), we have data $\mathscr{D}f(\alpha, \varphi)$ only for $\alpha \in [0, \alpha_0]$ corresponding to the limited angular range of sources and for $\varphi \in [\phi_0, \phi_1]$ where $\phi_0$ and $\phi_1$ correspond to the angle $\varphi$ from the source to the inner radius of the annulus, and $\phi_1$ is the angle to the outer radius. The author's algorithm needs to extend the data to use (3.8). We extended in $\varphi$ as above. We first tried to extend in $\alpha$ by smoothly tapering the data to 0 at $\alpha = 0$ and at $\alpha = \alpha_0$. This caused some distortion at the boundaries of the reconstruction and was not as successful for our data set as the following method. We altered (3.8) to integrate with respect to $\alpha$ only between 0 and $\alpha_0$, the limits of sources for the data, and this worked well without any smoothing or averaging. In [28] this data were extended linearly in $\alpha$ between $\alpha_0$ and $2\pi \sim 0$ for the author's exterior reconstruction algorithm, but this extra step does not seem to be necessary for Lambda Tomography, which is intrinsically local.

## 5. Reconstructions

The author reconstructed these data sets using his exterior reconstruction algorithm (ERA) in [28] (see Section 2). In fact, in [28], satisfactory reconstructions were given for $\frac{1}{32}$ the data used in Figs. 2 and 3. When one compares the Lambda reconstructions in Figs. 2 and 3 with those in [28] from the ERA, both Lambda reconstructions have better defined boundaries than the ones from the ERA [28]. However, the ERA reconstructions are more uniform inside each region, and the ERA provides accurate density values.

When looking at the reconstructions in Figs. 2 and 3, it is important to remember that the reconstructions are given in polar coordinates with $r$ along the vertical axis (with the outside of the object at the bottom) and $\theta$ on the horizontal. Furthermore, the $r$-axis (vertical) has been magnified by 25 times in Figs. 2 and 3. Thus the boundaries of the rocket shell mockup would be more uniform if to scale, and the small features (the little "box" in the center right of Fig. 2 and the four "W" objects in Fig. 3) would be much thinner.

These reconstructions illustrate the principle of Theorem 2. Essentially all the boundaries in the pictures are tangent to lines in the data set since they are more-or-less radial. One can assume that many rocket defects, including cracks and air bubbles between the insulation and shell will be of this nature, and this suggests that exterior tomography could be effective for the nondestructive evaluation of rockets and other large objects.

The horizontal bands in Fig. 2 could be related to detector normalizations since they correspond to specific detectors. The bands near the top of the pictures are not related to the data completion method (even though they are at the inside boundary of the data set) because they occur even when data are used farther into the object. The horizontal curve in the lower left of Fig. 3 could be a crack.

Finally, one main point of this article is to show that Lambda Tomography is adaptable to many limited data problems if one makes sure the data extension step does not add or eliminate singularities.

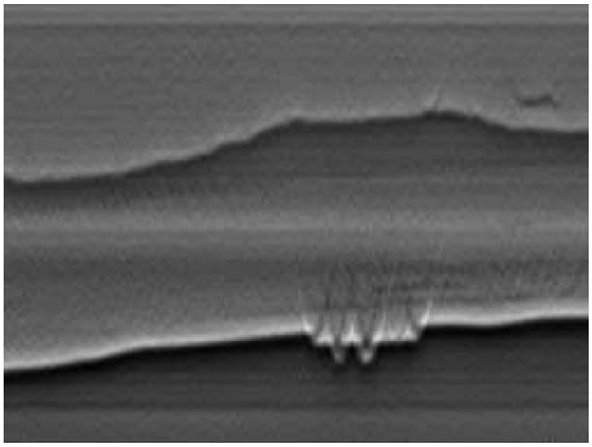

Fig. 2. Polar coordinate display of the author's exterior Lambda reconstruction from complete exterior data of a Perceptics rocket motor mockup. The horizontal axis corresponds to one-quarter of the circle, $\theta \in [0, \pi/2]$, the vertical corresponds to $r \in [0.9532, 1]$ (with $r = 1$ at the bottom and magnified by a factor of 25). Data were taken on 1800 evenly spaced source positions and 388 detectors.

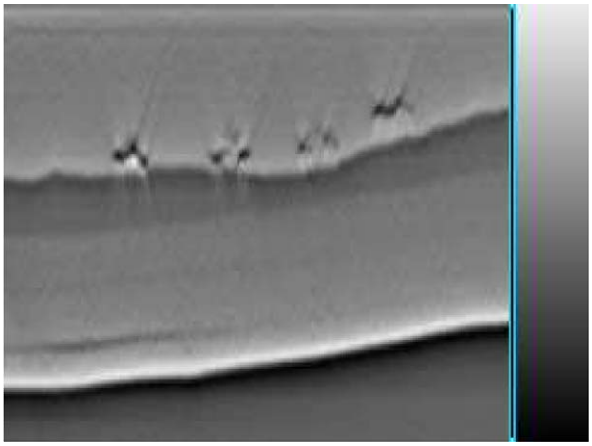

Fig. 3. Polar coordinate display of the author's limited angle exterior Lambda reconstruction from a $3\pi/4$ angular range limited angle exterior data set of a Perceptics rocket motor mockup. The horizontal axis corresponds to $\theta \in [0, \pi/2]$, the vertical corresponds to $r \in [0.9453, 1.0]$ (with $r = 1$ at the bottom and magnified by a factor of 25). Data were taken over 1350 sources in the range $[0, 3\pi/4]$ and 280 detectors.

## Acknowledgements

The author is indebted to Adel Faridani for many discussions over the years on Lambda Tomography and for showing the author his Lambda Tomography program. The author thanks Jim Youngberg, his scientific officer at Perceptics, for being a pleasure to work with and for providing the data (from which ERA reconstructions were previously published in [28]). This research is based upon work supported by the National Science Foundation under Grants DMS 0200788 and DMS 0456858 and Tufts University FRAC.

## References

[1] R. Bates, R. Lewitt, Image reconstruction from projections: I: general theoretical considerations, II: projection completion methods (theory) III: projection completion methods (computational examples), Optik 50 (1978) I: 19–33, II: 189–204, III: 269–278.
[2] E. Candès, L. Demanet, Curvelets and Fourier integral operators, C. R. Math. Acad. Sci. Paris Ser. I 336 (2003) 395–398.
[3] E. Candès, D.L. Donoho, Curvelets and reconstruction of images from noisy Radon data, in: M.A.U.A. Aldroubi, A.F. Laine (Eds.), Wavelet Applications in Signal and Image Processing VIII, Proceedings SPIE, vol. 4119, 2000.

[4] A.M. Cormack, Representation of a function by its line integrals with some radiological application, J. Appl. Phys. 34 (1963) 2722–2727.
[5] A.M. Cormack, Representation of a function by its line integrals with some radiological applications II, J. Appl. Phys. 35 (1964) 2908–2913.
[6] M. Davison, F. Grünbaum, Tomographic reconstruction with arbitrary directions, Comm. Pure Appl. Math. 34 (1981) 77–120.
[7] A. Faridani, D. Finch, E.L. Ritman, K.T. Smith, Local tomography, II, SIAM J. Appl. Math. 57 (1997) 1095–1127.
[8] A. Faridani, F. Keniert, F. Natterer, E.L. Ritman, K.T. Smith, Local and global tomography, in: Signal Processing, Part II, IMA Volumes in Mathematics and Applications, vol. 23, Springer, Berlin, 1990, pp. 241–255.
[9] A. Faridani, E.L. Ritman, K.T. Smith, Local tomography, SIAM J. Appl. Math. 52 (1992) 459–484.
[10] V. Guillemin, S. Sternberg, Geometric Asymptotics, American Mathematical Society, Providence, RI, 1977.
[11] L. Hörmander, Fourier integral operators, I,, Acta Math. 127 (1971) 79–183.
[12] P. Kuchment, K. Lancaster, L. Mogilevskaya, On local tomography, Inverse Problems 11 (1995) 571–589.
[13] A.K. Louis, Ghosts in tomography, the null space of the Radon transform, Math. Methods Appl. Sci. 3 (1981) 1–10.
[14] A.K. Louis, Incomplete data problems in X-ray computerized tomography I. Singular value decomposition of the limited angle transform, Numer. Math. 48 (1986) 251–262.
[15] A.K. Louis, A. Rieder, Incomplete data problems in X-ray computerized tomography II. Truncated projections and region-of-interest tomography, Numer. Math. 56 (1986) 371–383.
[16] W. Madych, Tomography, approximate reconstruction, and continuous wavelet transforms, Appl. Comput. Harmon. Anal. 7 (1999) 54–100.
[17] W.R. Madych, S.A. Nelson, Polynomial based algorithms for computed tomography, SIAM J. Appl. Math. 43 (1983) 157–185.
[18] F. Natterer, Efficient implementation of 'optimal' algorithms in computerized tomography, Math. Methods Appl. Sci. 2 (1980) 545–555.
[19] F. Natterer, The mathematics of computerized tomography, Classics in Mathematics, Society for Industrial and Applied Mathematics, New York, 2001.
[20] F. Natterer, F. Wübbeling, Mathematical Methods in Image Reconstruction, Monographs on Mathematical Modeling and Computation, Society for Industrial and Applied Mathematics, New York, 2001.
[21] R.M. Perry, On reconstructing a function on the exterior of a disc from its Radon transform, J. Math. Anal. Appl. 59 (1977) 324–341.
[22] B. Petersen, Introduction to the Fourier Transform and Pseudo-Differential Operators, Pittman, Boston, 1983.
[23] V. Pickalov, A. Likhachov, G. Fuchs, A. Ohl, G. Röttig, I. Bandlow, Region-of-interest tomography of fine structures in plasmas, in: Proceedings of the 1998 ICPP and 25th EPS Conference, vol. 22, Prague, 1998, Center for Fusion and Plasma Physics, Avon Books, New York, pp. 1570–1573.
[24] E.T. Quinto, The dependence of the generalized Radon transform on defining measures, Trans. Amer. Math. Soc. 257 (1980) 331–346.
[25] E.T. Quinto, Singular value decompositions and inversion methods for the exterior Radon transform and a spherical transform, J. Math. Anal. Appl. 95 (1983) 437–448.
[26] E.T. Quinto, Tomographic reconstructions from incomplete data-numerical inversion of the exterior Radon transform, Inverse Problems 4 (1988) 867–876.
[27] E.T. Quinto, Singularities of the X-ray transform and limited data tomography in $\mathbb{R}^2$ and $\mathbb{R}^3$, SIAM J. Math. Anal. 24 (1993) 1215–1225.
[28] E.T. Quinto, Exterior and limited angle tomography in non-destructive evaluation, Inverse Problems 14 (1998) 339–353.
[29] J. Radon, Über die Bestimmung von Funktionen durch ihre Integralwerte langs gewisser Mannigfaltigkeiten, Ber. Verh. Sach. Akad. 69 (1917) 262–277.
[30] A. Ramm, Inversion of limited-angle tomographic data, Comput. Math. Appl. 22 (1991) 101–111.
[31] A.G. Ramm, A. Katsevich, The Radon Transform and Local Tomography, CRC Press, Boca Raton, FL, 1996.
[32] F. Rashid-Farrokhi, K. Liu, C.A. Berenstein, D. Walnut, Wavelet-based multiresolution local tomography, IEEE Trans. Image Process. 6 (1997) 1412–1430.
[33] L.A. Shepp, S. Srivastava, Computed tomography of PKM and AKM exit cones, AT&T Tech. J. 65 (1986) 78–88.
[34] K.T. Smith, Inversion of the X-ray transform, SIAM-AMS Proc. 14 (1984) 41–52.
[35] E. Vainberg, I.A. Kazak, V.P. Kurozaev, Reconstruction of the internal three-dimensional structure of objects based on real-time integral projections, Soviet J. Nondestructive Testing 17 (1981) 415–423.